ISSN 1054-660X, Laser Physics, 2006, Vol. 16, No. 2, pp. 385–392.

Measuring the Photon Distribution with ON/OFF Photodetectors

M. Genovese[1, *], M. Gramegna[1], G. Brida[1], M. Bondani[2], G. Zambra[2], A. Andreoni[2], A. R. Rossi[3], and M. G. A. Paris[3]

[1] *Istituto Elettrotecnico Nazionale, IEN, Galileo Ferraris, Torino, Italia*

[2] *Istituto Nazionale per la Fisica della Materia, INFM and Dipartimento di Fisica e Matematica, Università degli Studi dell'Insubria, Como, Italia*

[3] *Dipartimento di Fisica dell' Università di Milano, Italia*

*e-mail: genovese@ien.it

Received July 8, 2005

Abstract—Reconstruction of photon statistics of optical states provides fundamental information on the nature of any optical field and helps with various relevant applications. Nevertheless, no detector that can reliably discriminate the number of incident photons is available. On the other hand, the alternative of reconstructing the density matrix by quantum tomography leads to various technical difficulties that are particularly severe in the pulsed regime (where mode matching between a signal and local oscillator is very challenging). Even if on/off detectors, as usual avalanche photodiodes operating in Geiger mode, seem useless as photo-counters, it was recently shown how reconstruction of photon statistics is possible by considering a variable quantum efficiency. Here we present experimental reconstructions of photon number distributions of both continuous-wave and pulsed light beams in a scheme based on on/off avalanche photodetection assisted by maximum-likelihood estimation. Reconstructions of the distribution for both semiclassical and quantum states of light (as single photon, coherent, pseudothermal, and multithermal states) are reported for single-mode and multimode beams. The stability and good accuracy obtained in the reconstruction of these states clearly demonstrate the interesting potentialities of this simple technique.

DOI: 10.1134/S1054660X06020320

1. INTRODUCTION

The evaluation of diagonal elements of the density matrix for quantum optical states, i.e., of the statistical distribution of the number of photons, provides fundamental information on the nature of any optical field and helps with various relevant applications, ranging from studies on the foundations of quantum mechanics [1] to quantum information [2] and quantum metrology. Despite the importance of photon distribution, photon detectors allowing an effective discrimination among different number of incident photons are not yet available. Among the possible candidates for number-resolving photodetectors, photomultiplier tubes (PMTs) [3] and hybrid photodetectors [4] have the drawback of a low quantum efficiency, since the detection starts with the emission of an electron from the photocathode. On the other hand, solid-state detectors with internal gain, in which the nature of the primary detection process ensures higher efficiency, are still under development. Highly efficient thermal photon counters have also been used. However, since they operate in cryogenic conditions, they are far from common use [5, 6]. Furthermore, their efficiency is limited by the optical window for entering the cryostat.

Quantum tomography provides an alternative method for measuring photon number distributions [9]. However, the tomography of a state, which has been applied to several quantum states [10], requires the implementation of homodyne detection, which in turn requires the appropriate mode matching of the signal with a suitable local oscillator at a beam splitter. In general, therefore, this technique is not simple to implement; in particular, such mode matching is a very challenging task in the case of pulsed optical fields.

On the other hand, the photodetectors usually employed in quantum optics, such as avalanche photodiodes (APDs) operating in the Geiger mode [6, 11] (which have relatively large quantum efficiencies), are not suited for distinguishing different numbers of incident photons, since they have the obvious drawback that the breakdown current is independent of the number of detected photons. The outcome of these APDs is either "off" (no photons detected) or "on," i.e., a "click" indicating the detection of one or more photons. Actually, such an outcome can be provided by any photodetector (PMT, hybrid photodetector, cryogenic thermal detector) for which the charge contained in dark pulses is definitely below that of the output current pulses corresponding to the detection of at least one photon. Notice that, for most high-gain PMTs, the anodic pulses corresponding to the "no photons" ("no click") event can be easily discriminated by a threshold from those corresponding to the detection of one or more

photons. On the other hand, as we will describe in the next paragraph, these detectors can be used for reconstructing photon statistics when measurements at different quantum efficiencies are performed.

In this paper, we present in some detail (see [8] for a shorter summary of these results) experimental reconstructions of photon number distributions of both continuous-wave and pulsed light beams in a scheme based on on/off avalanche photodetection assisted by maximum-likelihood estimation. Reconstructions of the distribution for both semiclassical and quantum states of light (as single photon, coherent, pseudothermal, and multithermal states) are reported for single-mode and multimode beams.

2. THEORETICAL METHOD

The statistics of the "no click" and "click" events from an on/off detector, assuming no dark counts, is given by

$$p_0(\eta) = \sum_n (1-\eta)^n \varrho_n, \qquad (1)$$

and $p_{>0}(\eta) = 1 - p_0(\eta)$, where $\varrho_n = \langle n|\varrho|n\rangle$ is the photon distribution of the quantum state ϱ and η is the quantum efficiency of the detector, i.e., the probability of a single photon to be revealed. At first sight, the statistics of an on/off detector appears to provide quite a scarce amount of information about the state under investigation. However, if the statistics about $p_0(\eta)$ is collected for a suitably large set of efficiency values, then the information is enough to reconstruct the whole photon distribution ϱ_n of the signal, upon a suitable truncation at $\bar{n}$ of the Hilbert space.

The reconstruction of photon distribution through on/off detection at different efficiencies has been analyzed [12] and its statistical reliability investigated in some detail [13]. In addition, the case of few and small values of η [14] has been addressed. However, whilst these theoretical studies found application in multichannel fiber loop detectors [15, 16], an experimental implementation of this technique for reconstructing photon distribution of a free-propagating field is still missing. In view of the relevance of photon distribution for applications in quantum information and the foundations of quantum mechanics, our purpose is to show that a reconstruction of the photon distribution by using this technique can be effectively realized gathering results obtained from measurement at different quantum efficiencies. As we will see, this method leads to excellent results both for free-propagating continuous-wave (CW) and pulsed light beams, for both single-mode semiclassical and quantum states, as well as for multimode states.

The procedure consists in measuring a given signal by on/off detection using different values η_ν ($\nu = 1, \ldots, K$) of the quantum efficiency. The information provided by experimental data is contained in the collection of frequencies $f_\nu = f_0(\eta_\nu) = n_{0\nu}/n_\nu$, where $n_{0\nu}$ is the number of "no click" events and n_ν the total number of runs with quantum efficiency η_ν. Then we consider expression (1) as a statistical model for the parameters ϱ_n to be solved by maximum-likelihood (ML) estimation. Upon defining $p_\nu \equiv p_0(\eta_\nu)$ and $A_{\nu n} = (1-\eta_\nu)^n$, we rewrite expression (1) as $p_\nu = \sum_n A_{\nu n}\varrho_n$. Since the model is linear and the parameters to be estimated are positive (LINPOS problem), then the solution can be obtained by using the expectation maximization algorithm (EM) [17]. By imposing the restriction $\sum_n \varrho_n = 1$, we obtain the iterative solution

$$\varrho_n^{(i+1)} = \varrho_n^{(i)} \sum_{\nu=1}^{K} \frac{A_{\nu n}}{\sum_\lambda A_{\lambda n}} \frac{f_\nu}{p_\nu[\{\varrho_n^{(i)}\}]}, \qquad (2)$$

where $p_\nu[\{\varrho_n^{(i)}\}]$ are the probabilities p_ν, as calculated using the reconstructed distribution $\{\varrho_n^{(i)}\}$ at the ith iteration.

Before going to the experimental implementation, we have performed several numerical simulations in order to check the accuracy and reliability of this method by varying the different parameters. Since the solution of the ML estimation is obtained iteratively, the most important aspect to keep under control is its convergence. Of course, the degree of convergence at a given step can be checked evaluating the log-likelihood function $\mathcal{L} = \log L$, $L = \prod_{\nu=1}^{K} p_\nu^{n_{0\nu}} (1-p_\nu)^{n_\nu - n_{0\nu}}$. However, a more suitable parameter is given by the total absolute error at the ith iteration, i.e.,

$$\varepsilon^{(i)} = \sum_{\nu=0}^{K} \left| f_\nu - p_\nu[\{\varrho_n^{(i)}\}] \right|. \qquad (3)$$

Indeed, the total error measures the distance of the probabilities $p_\nu[\{\varrho_n^{(i)}\}]$, as calculated at the ith iteration, from the actual experimental frequencies; thus, in addition to convergence, it quantifies how the estimated distribution reproduces the experimental data. The total distance is a decreasing function of the number of iterations. Its stationary value is proportional to the accuracy of the experimental frequencies $\{f_\nu\}$. For a finite data sample, this value is on the order of $1/\sqrt{n_\nu}$ for each value of η_ν, giving us a rough estimate of $\bar{n}/\sqrt{n_\nu}$ for the total error for the reconstructed probability $p_\nu[\{\varrho_n^{(i)}\}]$. If the stationary value of $\varepsilon^{(i)}$ is of this order, we have double-checked the convergence of the whole method. Notice that these properties are not shared by the log

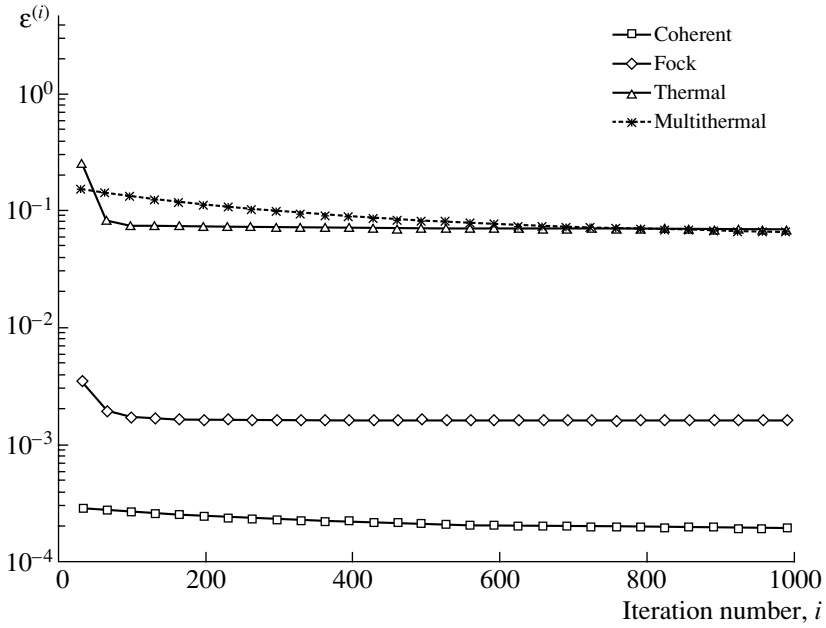

Fig. 1. Plot of the total error $\varepsilon^{(i)}$ as a function of the iteration number for the various states of the field (corresponding to the states experimentally investigated; see next sections). For the thermal distribution, the value of the total error is plotted at each iteration step (value on the x axis), while for the other states the value of $\varepsilon^{(i)}$ is the average over an suitable set of iterations.

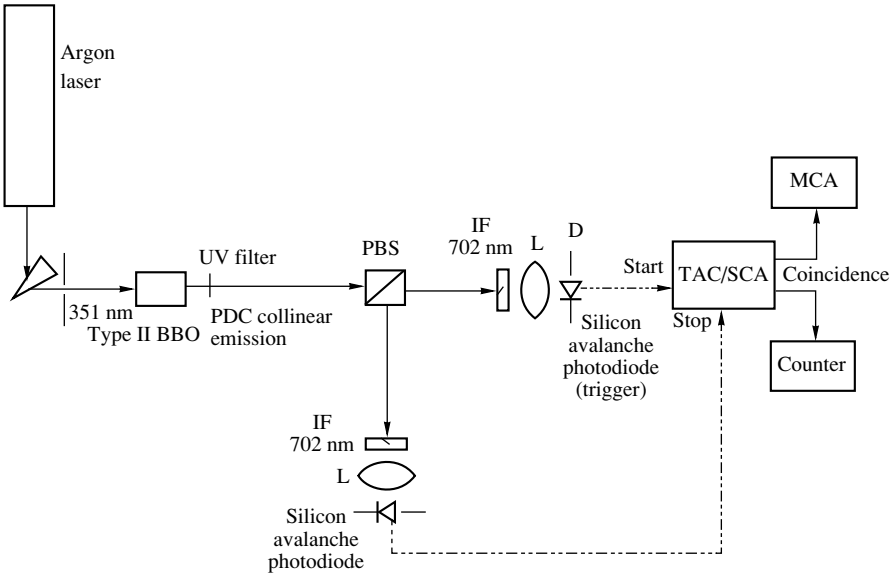

Fig. 2. Setup for heralded single PDC photon reconstruction. An Ar^+ laser beam pumps a type II BBO crystal generating collinear degenerate PDC. After an anti-UV filter, pairs are split on a PBS. Observation of a photon on trigger detector D (preceded by a lens, L, and an interference filter IF) starts a TAC ramp, which is eventually closed by a stop signal deriving from the observation of a photon in the second detector.

likelihood: its stationarity certainly reveals convergence, but the value depends on the statistics to be retrieved and so cannot even be estimated by *a priori* considerations.

In order to check the convergence of the iterations in (2), we run simulated experiments to reconstruct some of the states subsequently investigated experimentally (see the next sections and Figs. 3–7). The results are

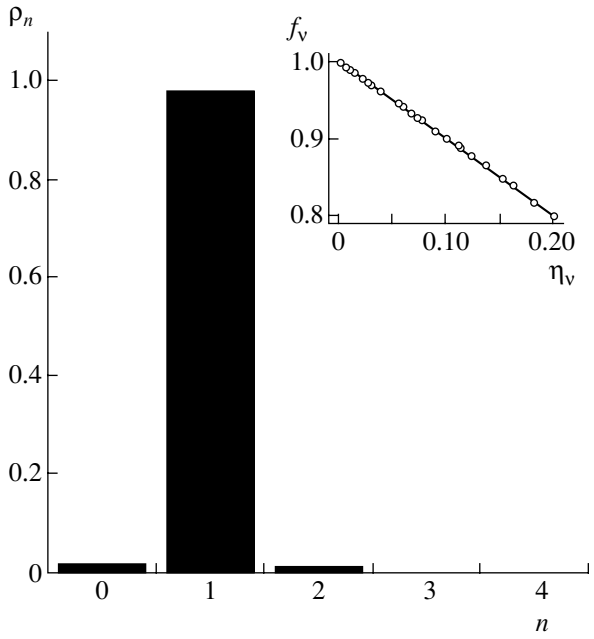

Fig. 3. Reconstruction of the photon distribution for the heralded single-photon state produced in spontaneous type II PDC. Inset: Experimental frequencies f_ν of no-click events as a function of the quantum efficiency η_ν for a PDC heralded photon state compared with the theoretical curve $p_\nu = 1 - \eta_\nu$.

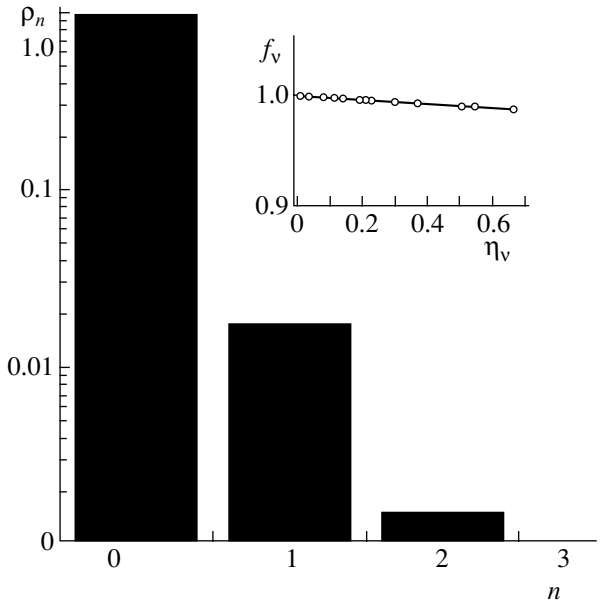

Fig. 4. Reconstruction of the photon distribution for a weak coherent state. In the inset, the experimental frequencies f_ν of no-click events as a function of the quantum efficiency η_ν for a PDC heralded photon state are compared with a typical curve for a weak coherent beam $p_\nu \simeq 1 - \eta_\nu|\alpha|^2$.

shown in Fig. 1, where the total error (ratio of its stationary value) is reported as a function of the number of iterations. As is apparent from the plot, the total error shows a transient behavior and then quickly converges to its stationary value. The rate of convergence depends on the signal under investigation. Our results show that the iterative algorithm always converges, and the asymptotic value of $\varepsilon^{(i)}$ is of the expected order of magnitude.

An estimate of the confidence interval on the determination of the element ϱ_n can be given in terms of the variance

$$\sigma_n = (\mathcal{N} F_n)^{-1/2}, \tag{4}$$

where $\mathcal{N}$ is the total number of measurements and F_n is the Fisher information [7]

$$F_n = \sum_\nu \frac{1}{q_\nu}\left(\frac{\partial q_\nu}{\partial \varrho_n}\right)^2, \tag{5}$$

where

$$q_\nu = \frac{p_\nu}{\sum_\nu p_\nu} = \frac{\sum_n A_{\nu n}\varrho_n}{\sum_{\nu n} A_{\nu n}\varrho_n} \tag{6}$$

represents the renormalized probabilities of the *no-click* event at quantum efficiency η_ν.

3. EXPERIMENTAL DATA IN CW REGIME

In the following, we present various different applications of this method to both the CW and pulsed regimes, with the purpose of demonstrating the potentialities of this technique. For what concerns CW regime, we have studied reconstruction of the diagonal element of the density matrix for single-photon Fock states and a weak coherent one.

The single photon states have been generated by producing parametric down conversion (PDC) heralded photons. In more detail (see Fig. 2), pairs of correlated photons have been generated by pumping in collinear degenerate geometry a 5-mm-long β-barium borate (BBO) crystal, cut for type-II phase matching (i.e., the two photons of the pair have orthogonal polarizations), with a 0.3-W CW argon ion laser beam with a wavelength of 351 nm. The heralded single-photon scheme is based on the specific properties of PDC emission. PDC is a quantum effect without classical counterparts and consists of the spontaneous decay inside a nonlinear crystal of one photon from a pump beam (usually generated by a laser) into a couple of photons conventionally called signal and idler. This decay process obeys (phase matching laws) energy conservation

$$\omega_0 = \omega_i + \omega_s \tag{7}$$

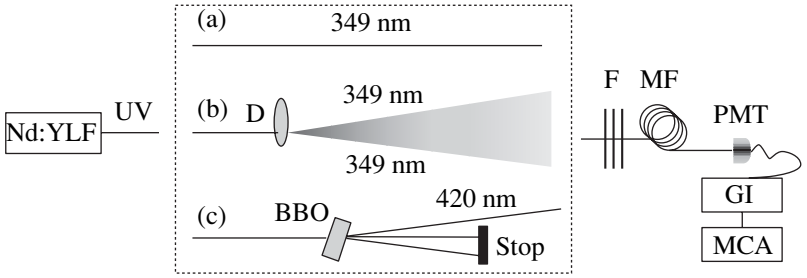

Fig. 5. Setup for the generation of pulsed optical states. Starting with the third-harmonics of a Nd:YLF laser, we obtain: (a) Gaussian state; (b) thermal state; (c) multithermal state. D, rotating ground-glass diffuser; BBO, type-I nonlinear crystal; F, variable filter; MF, multimode fiber; PMT, photomultiplier detector; GI, gated integrator; MCA, multichannel analyzer.

and momentum conservation

$$\mathbf{k}_0 = \mathbf{k}_i + \mathbf{k}_s, \tag{8}$$

where ω_0, ω_i, ω_s are the frequencies and $\mathbf{k}_0$, $\mathbf{k}_i$, $\mathbf{k}_s$ are the wave vectors of pump, idler, and signal photon, respectively. Furthermore, the two photons are produced, within a few tens of femtoseconds, at the same time. The probability of a spontaneous decay into a pair of correlated photons is usually very low, on the order of 10^{-9} or lower; therefore, with a typical pump power on the order of several milliwatts, the fluorescence emission lies at the levels of the photon counting regime. Since the photons are produced in pairs and because of the energy and momentum conservation restrictions, the detection of one photon in a certain direction and with a given energy indicates the existence of the pair-correlated one, with definite energy in a well-defined direction. This property allows "heralding" of the second photon of the pair once the first one is detected in a precise direction (and temporal and spectral window). This "heralded photon" was the state to be measured. In our setup, having eliminated the pump laser beam with a filter, the two photons of the pair are separated by means of a polarizing beam splitter. The detection of one photon in one of the two conjugated directions was then used to open a window of $\Delta t = 4.9$ ns for detection in arm 2. This was realized by addressing the first detection signal as the start to a time-to-amplitude converter (TAC); the signal from the second detector (after a delay line) was then addressed to the same TAC as a stop and counted only if arriving in a window of Δt.

The photodetection apparatuses were constituted by a silicon avalanche photodiode detector preceded by an iris and an interference filter (IF) at 702 nm, 4 nm FWHM, inserted with the purpose of reducing the stray light. Both detectors were silicon avalanche photodiode detectors (SPCM-AQR-15, Perkin Elmer). The quantum efficiency of the "heralded photon" detection apparatus (including IF and iris) was measured to be 20% by using the standard calibration scheme based on correlation properties of PDC emission (see [18]). Lower quantum efficiencies, needed for the reconstruction scheme, were simulated by inserting calibrated neutral density filters on the optical path. A comparison of the observed frequencies f_ν with the theoretical curve $(1 - \eta_\nu)$ is presented in the inset of Fig. 3. The photon distribution has been reconstructed using $K = 34$ different values of the quantum efficiency from $\eta_\nu \simeq 0.01\%$ to $\eta_\nu \simeq 20\%$ with $n_\nu = 10^6$ runs for each η_ν. Results at iteration $i = 10^6$ are shown in Fig. 3. As expected, the PDC heralded photon state largely agrees with a single-photon Fock state. However, a small two-photon component and a vacuum one are also observed. The ρ_2 contribution is expected, by estimating the probability that a second photon randomly enters the detection window, to be 1.85% of ρ_1, in agreement with what is observed. A nonzero ρ_0 is also expected due to background. This quantity can be evaluated by measuring the counts when the polarization of the pump beam is rotated by a

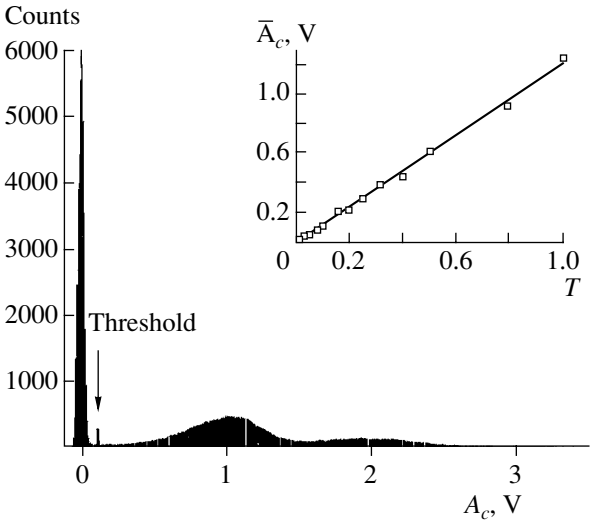

Fig. 6. Histogram of the detected anodic charge of the PMT (data corresponding to the measurement of a Gaussian field having $N = 4.88$ with $\eta = 0.20$). The arrow indicates the threshold value used to discriminate on/off events. Inset: linearity test for the PMT detector: mean anodic current as a function of the transmittance of calibrated filters.

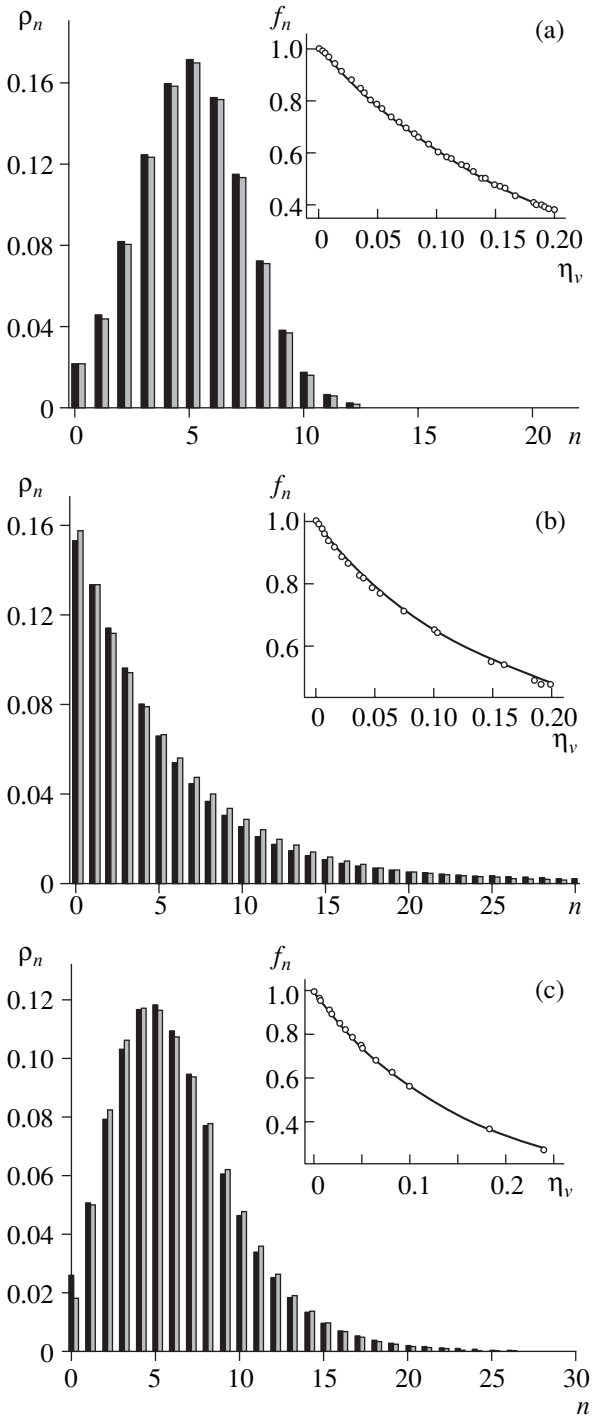

Fig. 7. Reconstructed photon distribution (black bars) and best theoretical fit (gray bars) for three different states in the pulsed regime: (a) laser pulse, (b) diffused laser pulse, (c) multimode state produced in type-I PDC. Insets: Experimental frequency f_ν data in function of the quantum efficiency η_ν and theoretical model for each one of the states.

λ/2 wave plate to avoid generation of parametric fluorescence. In this case as well, our estimate, (2.7 ± 0.2)%, is in good agreement with the reconstructed ρ_0.

As a second example, we have reconstructed the statistics of a strongly attenuated coherent state, which has been produced by a He–Ne laser beam attenuated to the photon-counting regime by insertion of neutral filters. The same silicon avalanche photodiode detector of the previous case was used here as well. The counts were measured in about a 400-ns window obtained by gating the photodetector with a periodic signal (10 kHz rate). It must be noted that, in this case, we do not have interference filters or irises in front of the detector and all the other attenuations can be included in the generation of the state (i.e., they contribute to the absorption together with neutral filters); thus, the highest quantum efficiency is assumed to be 66%, as declared by the manufacturer data sheet for the photodetector. The reconstructed distribution, with $K = 15$ different values of the quantum efficiency from $\eta_\nu \simeq 0.1$ to ≃66% with $n_\nu = 10^6$ runs for each η_ν, agrees well with what is expected for a coherent state with the average number of photons $|\alpha|^2 \simeq 0.02$. Figure 4 shows both the frequencies f_ν as a function of η_ν compared with the theoretical prediction $p_\nu = \exp\{-\eta_\nu|\alpha|^2\} \simeq 1 - \eta_\nu|\alpha|^2$ and the reconstructed photon statistics. Finally, we briefly acknowledge that a comparable result was also obtained with a very strongly attenuated thermal state, i.e., light emitted by a thermal source, a tungsten lamp attenuated by neutral density filters.

4. EXPERIMENTAL DATA IN PULSED REGIME

In the pulsed domain, we measured three different optical states generated starting from the third harmonics (349 nm, 4.45 ps) of a CW mode-locked Nd : YLF laser regeneratively amplified at a repetition rate of 500 Hz (High Q Laser). The general experimental setup is shown in Fig. 5. For all the measurements, the light was delivered to a photomultiplier tube (PMT, Burle 8850) through a multimode fiber (100 μm core diameter). Although the PMT has the capability of counting the number of photoelectrons produced by one or more photons [3], for the present application we used it in a Geiger-like configuration, by setting a threshold to discriminate on/off events. Furthermore, we take advantage of the linearity of the mean anodic charge, $\overline{A^c}$ (see inset in Fig. 6), as a function of the mean energy of the measured light [20] to obtain the values of η_ν. In fact, if we set $\overline{A^c} = 0$ for $\eta = 0$ and $\overline{A^c} = (\overline{A^c})_{\max}$ for $\eta = \eta_P$ (nominal quantum efficiency of the PMT), for all the intermediate quantum efficiencies obtained by attenuating the light with neutral filters, we have $\eta = (\eta_P/(\overline{A^c})_{\max})\overline{A^c}$. This procedure allow us to continuously vary the quantum efficiency.

The first measurement was performed on the pulse emerging from the laser source. Due to the pulsed nature of the source, we do not expect to recover a true Poissonian statistics as in the CW measurement

described above. Rather, we expect a Gaussian distribution of the form [21]

$$\varrho_{n,G} = \frac{1}{\sqrt{2\pi(N+\sigma^2)}}\exp\left[-\frac{(n-N)^2}{2(N+\sigma^2)}\right], \qquad (9)$$

which takes into account the presence of noise; N is the photon mean value and σ^2/N can be taken as a measure of the deviation from Poissonian statistics. In Fig. 7a, we show the photon distribution ϱ_n, reconstructed at the $i = 50000$ iteration of the ML algorithm, along with the best fit obtained with the model (9) (fitting parameters $N = 4.88$ and $\sigma^2 = 0.63$). The inset of the figure compares the experimental frequency f_ν data ($K = 37$ values of η, $n_\nu = 10^4$ runs for each η) as a function of η_ν with the theoretical values calculated through (1) and the parameters given by the fit of the photon distribution. Both the reconstructed distribution and the experimental frequencies agrees very well with the above Gaussian model. The fidelity of the reconstruction is $G \simeq 0.998$. Using the estimated value of σ^2, a deviation of about 13% of the laser photon number distribution from the Poissonian statistics can be derived.

A second measurement was performed on the laser pulse diffused by a moving ground glass. When the photons are collected from within an area of spatial coherence, the system acts as a pseudothermal source, whose photon number distribution satisfies

$$\varrho_{n,T} = \frac{N^n}{(N+1)^{n+1}}. \qquad (10)$$

Figure 7b shows the photon distribution ϱ_n, as reconstructed at the $i = 400$ iteration and the best fit of the data with (10) ($N = 5.33$); the fidelity is given by $G \simeq 0.995$. The inset of the figure contains the experimental frequency f_ν data ($K = 24$ values of η, $n_\nu = 10^4$ runs for each η) and their theoretical values as calculated from (1).

The last measurement was performed on the blue portion (420 nm) of the down-conversion fluorescence produced by a type I BBO crystal (10 mm depth, cut at 34°) pumped by the laser pulse. The pump, incident orthogonally to the crystal face, had an intensity ~60 GW/cm^2. Under these experimental conditions, we expect a coherence time of the generated field of ~1 ps, which corresponds to measuring a convolution of 4–5 temporal modes [19]. The photon number distribution is expected to be a "multithermal" distribution of the form

$$\varrho_{n,M} = \frac{(n+\mu-1)!}{n!(\mu-1)!(1+N/\mu)^n(1+\mu/N)^\mu}, \qquad (11)$$

where μ is the number of temporal modes. The photon distribution reconstructed at the $i = 1500$ iteration is shown in Fig. 7c along with the best fit of the data using (11) ($N = 6.17$ and $\mu = 5$); the fidelity of the reconstruction is given by $G \simeq 1$. In the inset of the figure, we show the experimental frequency f_ν data ($K = 18$ values of η, $n_\nu = 10^4$ runs for each η) and their theoretical values as calculated according to (1). As a comment to the experimental results in the pulsed regime, we note that the best reconstruction of the photon distribution is achieved at a different number of iterations for the three different measured optical states, and that the absolute error ε does not approach the same value. This is due to the presence of excess noise in our measurements, since the stability and the repetition rate of our source (500 Hz) limits to $n_\nu \sim 10^4$ the number of runs for each value of the quantum efficiency [13]. The choice of the best iteration to stop the algorithm is driven by the possibility to fit the distribution with a suitable model. We stress that there was no *a priori* decision in choosing a Gaussian distribution for case (a) or of a multithermal distribution for case (c), but, on the contrary, we followed the *a posteriori* observation that no other distribution could fit equally well the reconstructed data.

5. CONCLUSIONS

In summary, we have presented experimental results on the reconstruction of the photon distribution based on on/off detection at different quantum efficiency followed by a maximum-likelihood iterative algorithm based on the theoretical analysis presented in [13].

Our results concern single-photon (PDC-heralded) and weak coherent states in the CW regime, as well as coherent, thermal, and multithermal states in the pulsed regime. The stability and the good accuracy shown in the reconstruction of these states, together with the simplicity of the method, clearly demonstrate the interesting potentialities of this technique, suggesting relevant future applications including studies on quantum optics, the foundations of quantum mechanics, quantum information, and quantum metrology. Some applications in these fields are now being realized in our laboratories (reconstruction of further quantum optical states and of entangled states [22], characterization of a high spectral selection heralded photon source [23], etc.).

ACKNOWLEDGMENTS

This work was supported by MIUR (FIRB RBAU01L5AZ-002 and RBAU014CLC-002), INFM (PRA-CLON), "Regione Piemonte," and Fondazione San Paolo. A.R. and M.G.A.P. thank Stefano Olivares for many fruitful discussions.

REFERENCES

1. M. Genovese, Phys. Rep. **413-6**, 319 (2005).
2. M. A. Nielsen and I. L. Chuang, *Quantum Computation and Quantum Information* (Cambridge Univ. Press, Cambridge, 2000); D. Bouwmeester, A. Ekert, and A. Zeilinger, *The Physics of Quantum Information* (Springer, Berlin, 2000).

3. G. Zambra, M. Bondani, A. S. Spinelli, and A. Andreoni, Rev. Sci. Instrum. **75**, 2762 (2004).
4. E. Hergert, *Single Photon Detector Workshop* (NIST, Gaithersburg, 2003).
5. J. Kim, S. Takeuchi, Y. Yamamoto, and H. H. Hogue, Appl. Phys. Lett. **74**, 902 (1999); A. Peacock, P. Verhoeve, N. Rando, Nature **381**, 135 (1996).
6. G. Di Giuseppe, A. V. Sergienko, B. E. A. Saleh, and M. C. Teich, "Quantum Information and Computation," Proc. SPIE **5105**, 39 (2003).
7. H. Cramer, *Mathematical Methods of Statistics* (Princeton Univ. Press, Princeton, 1946).
8. M. Bondani, *et al.*, quant-ph/0502060; Phys. Rev. Lett. (in press).
9. M. Munroe, D. Boggavarapu, M. E. Anderson, and M. G. Raymer, Phys. Rev. A **52**, R924 (1995); Y. Zhang, K. Kasai, and M. Watanabe, Opt. Lett. **27**, 1244 (2002).
10. M. Raymer and M. Beck, *Quantum States Estimation*, Ed. by M. G. A. Paris and J. Řeháćek (Springer, Heidelberg, 2004).
11. F. Zappa, A. L. Lacaita, S. D. Cova, and P. Lovati, Opt. Eng. **35**, 938 (1996); D. Achilles, C. Silbergorn, C. Śliwa, K. Banaszek, and I. A. Walmsley, Opt. Lett. **28**, 2387 (2003).
12. D. Mogilevtsev, Opt. Comm. **156**, 307 (1998); Acta Phys. Slov. **49**, 743 (1999).
13. A. R. Rossi, S. Olivares, and M. G. A. Paris, Phys. Rev. **70**, 055801 (2004).
14. A. R. Rossi and M. G. A. Paris, Eur. Phys. J. D **32**, 223 (2005).
15. J. Řeháćek, Z. Hradil, O. Haderka, *et al.*, Phys. Rev. A **67**, 061801(R) (2003); O. Haderka, M. Hamar, and J. Perina, Eur. Phys. J. D **28**, (2004).
16. K. Banaszek and I. A. Walmsley, Opt. Lett. **28**, 52 (2003).
17. A. P. Dempster, N. M. Laird, and D. B. Rubin, J. R. Stat. Soc. B **39**, 1 (1977); Y. Vardi and D. Lee, J. R. Stat. Soc. B **55**, 569 (1993); R. A. Boyles, J. R. Stat. Soc. B **45**, 47 (1983).
18. G. Brida, M. Genovese, and C. Novero, J. Mod. Opt. **47**, 2099 (2000); G. Brida, M. Genovese and M. Gramegna, Laser Phys. (in press).
19. F. Paleari, A. Andreoni. G. Zambra, and M. Bondani, Opt. Express **13**, 2816 (2004).
20. G. F. Knoll, *Radiation, Detection and Measurement* (John Wiley and Sons, New York, 1989).
21. R. Loudon, *The Quantum Theory of Light* (Oxford Unive. Press, New York, 2000).
22. G. Brida, *et al.*, Phys. Lett. A **268**, 12 (2000); Phys. Lett. **299**, 121 (2002); Phys. Rev. A **70**, 032332 (2004).
23. M. Genovese, *et al.*, Opt. Spectrosc. **99**, 185 (2005).